

Meta-Learning Neural Process for Implied Volatility Surfaces with SABR-induced Priors

Jirong Zhuang^a, Xuan Wu^{*a}

^a*Department of Mathematics, University of Macau, Avenida da Universidade Taipa, 999078, Macau, China*

Abstract

Constructing the implied volatility surface (IVS) is reframed as a meta-learning problem—training across trading days to learn a general process that reconstructs a full IVS from few quotes, eliminating daily recalibration. We introduce the Volatility Neural Process, an attention-based model that uses a two-stage training: pre-training on SABR-generated surfaces to encode a financial prior, followed by fine-tuning on market data. On S&P 500 options (2006–2023; out-of-sample 2019–2023), our model outperforms SABR, SSVI, Gaussian Process, and an ablation trained only on real data. Relative to the ablation, the SABR-induced prior reduces RMSE by about 40% and dominates in mid- and long-maturity regions where quotes are sparse. The learned prior suppresses large errors, providing a practical, data-efficient route to stable IVS construction with a single deployable model.

Keywords:

Implied volatility surface, Meta-learning, Neural process, Transfer learning

1. Introduction

Constructing the implied volatility surface (IVS) is a fundamental task in quantitative finance, essential for derivative pricing and risk management. A popular class of approaches are structural models (e.g., the SABR model (Hagan et al., 2002), Heston model (Heston, 1993)) and related parametric models (Gatheral, 2004; Gatheral and Jacquier, 2014). These models typically assume that the volatility of the underlying asset follows a stochastic differential equation and are effective at capturing the general shape of the volatility smile. However, their fixed mathematical forms can be overly rigid, failing to capture more complex market patterns. Another class of approaches are data-driven methods like Gaussian Process regression (De Spiegeleer et al., 2018; Roberts and Tegnér, 2021). These methods offer greater flexibility, but are prone to overfitting sparse and noisy market data, leading to financially implausible surfaces (e.g., admitting arbitrage opportunities). A common challenge of both approaches is that they treat each trading day as an isolated fitting problem, requiring daily recalibration.

This limitation motivates reframing the problem as a meta-learning task: by “meta-learning” we mean training across day-level tasks to learn a procedure that reconstructs a full surface from few quotes on a new day, thereby avoiding per-day recalibration. We propose the Volatility Neural Process (VolNP), a Neural Process model (Garnelo et al., 2018b,a) designed to learn a general mapping from a sparse set of option quotes to a complete IVS. However, like other data-driven methods, Neural Processes are still prone to generating unstable and highly irregular surfaces in sparse market data. A growing body of work seeks to address this issue by incorporating financial knowledge into machine learning models, often through the imposition of constraints (e.g., no-butterfly arbitrage) derived from financial theory (Ackerer et al., 2020; Chataigner et al., 2021; Zheng et al., 2021; Hoshisashi et al., 2023; Wiedemann et al., 2025; Vuletić and Cont, 2024).

In contrast to these constraint-based methods, our approach integrates transfer learning (Chen et al., 2023). The model is first pre-trained on surfaces generated from structural models. This stage instills a prior for the shape of a financially plausible implied volatility surface into the model. Then the model is

fine-tuned on real market data, enabling it to adapt this prior to complex market dynamics. This two-stage training enhances VolNP’s ability to reduce prediction errors and produce consistent surfaces from sparse data.

The rest of this paper is organized as follows. Section 2 formulates the problem. Section 3 describes our model and training methodology. Section 4 presents the experimental results, and Section 5 concludes the paper.

2. Problem Formulation

On any given trading day q , the implied volatility surface (IVS) can be represented by a function $f_q : \mathbb{R}^2 \rightarrow \mathbb{R}^+$. This function maps a coordinate $\mathbf{x} = [k, \tau]^\top$ (log-moneyness and time-to-expiry) to its corresponding implied volatility y . We define log-moneyness as $k = \log(K/F_q)$, where F_q is the day q forward price. The function f_q is unobservable because only a finite set of quotes is available. Traditional methods address this by fitting a new model to these quotes each day, treating every f_q as an independent regression problem.

We formulate the IVS construction problem within a meta-learning framework. The goal of meta-learning is to train a single, universal model that learns the process of surface construction itself. Let $\mathcal{Q} = \{1, 2, \dots, Q\}$ be the set of available trading days. This model is trained on a distribution of learning tasks, where each task corresponds to constructing the IVS for a specific day $q \in \mathcal{Q}$. By learning from the wide variety of market conditions observed across \mathcal{Q} , the model is expected to construct a reliable implied volatility surface for a new day using only a small number of observed quotes.

A specific learning task for the model involves being given a sparse context set $\mathcal{D}_C = \{(\mathbf{x}_j, y_j)\}_{j=1}^N$, sampled from the market data of a single day $q \in \mathcal{Q}$, and being asked to reconstruct the entire surface f_q . Formally, the objective is to learn a single model that can use a context set \mathcal{D}_C to produce a predictive distribution $p(\tilde{y}|\tilde{\mathbf{x}}, \mathcal{D}_C)$ for any target coordinate $\tilde{\mathbf{x}}$.

3. Volatility Neural Process

3.1. Model Architecture

To address the set-to-function regression task defined within our meta-learning framework, we propose the Volatility Neural Process (VolNP) model which is a variant of the Attentive Neural Process (Kim et al., 2019). The following describes how the model processes the inputs for a single task. Such a task consists of a context set \mathcal{D}_C and a set of target coordinates \mathcal{X}_T . For notational simplicity, we will use these symbols throughout this subsection to refer to the inputs of a single forward pass of the model.

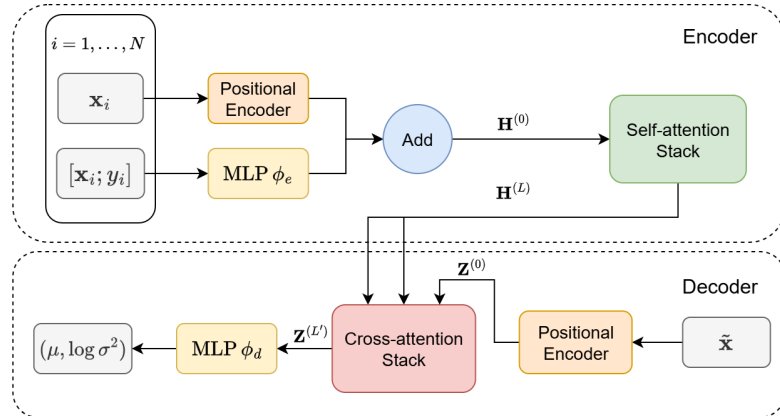


Figure 1: The architecture of the Volatility Neural Process (VolNP) model.

The model is an encoder-decoder architecture (see Figure 1) with attention mechanisms, designed to effectively model the complex interactions within a set of context points and reason about target predictions.

3.1.1. Encoder

The encoder's goal is to learn the complex relationships between the individual option quotes in the context set \mathcal{D}_C . It maps this set to a matrix of contextualized representations, $\mathbf{H}^{(L)} \in \mathbb{R}^{N \times d_r}$, where d_r is the hidden dimension, and each row contains a summary of a single point informed by all other points.

The process begins by creating an initial representation $\mathbf{h}_i^{(0)}$ for each context point (\mathbf{x}_i, y_i) :

$$\mathbf{h}_i^{(0)} = \phi_e([\mathbf{x}_i; y_i]) + \gamma(\mathbf{x}_i) \quad (1)$$

where $\phi_e : \mathbb{R}^3 \rightarrow \mathbb{R}^{d_r}$ is a learnable Multilayer Perceptron (MLP) and $[\cdot; \cdot]$ denotes concatenation. This step combines two types of information. First, ϕ_e extracts a set of features from the raw data. Second, we add a fixed sinusoidal positional encoding (Vaswani et al., 2017), $\gamma(\mathbf{x}_i)$. The resulting representation $\mathbf{h}_i^{(0)}$ thus contains information about both the specific value of an option quote and its absolute position on the moneyness-expiry grid. The collection of initial states forms the matrix $\mathbf{H}^{(0)} = [\mathbf{h}_1^{(0)}, \dots, \mathbf{h}_N^{(0)}]^\top$.

Next, these initial representations are processed by a stack of L self-attention blocks (SA). This is the core mechanism that allows the model to reason about the global structure of the volatility surface. A single option quote is only meaningful in the context of others; for instance, the implied volatility of an at-the-money option is intrinsically linked to its out-of-the-money counterparts, collectively forming the "smile" for a given maturity. The self-attention mechanism formalizes this intuition. It allows each point $\mathbf{h}_i^{(0)}$ to query all other points on the surface and update its representation based on their relationships. Through this process, the model learns to identify and encode complex, non-local patterns directly from the sparse data.

$$\mathbf{H}^{(l)} = \text{SA}(\mathbf{H}^{(l-1)}) \quad \text{for } l = 1, \dots, L \quad (2)$$

Each SA block is built around a Multi-Head Attention (MHA) mechanism (Vaswani et al., 2017) and uses a Pre-LayerNorm architecture (Xiong et al., 2020) for better training stability.

In this self-attention step, the Query (\mathbf{Q}), Key (\mathbf{K}), and Value (\mathbf{V}) matrices are all derived from the same input, $\mathbf{H}^{(l-1)}$. The model compares each option quote (Query) to all other quotes (Key) to decide how much information to draw from them (Value). The model performs this comparison not just once, but with n_h parallel "attention heads". Here, the projection matrices $\mathbf{W}_i^Q, \mathbf{W}_i^K \in \mathbb{R}^{d_r \times d_k}$, $\mathbf{W}_i^V \in \mathbb{R}^{d_r \times d_v}$, and $\mathbf{W} \in \mathbb{R}^{n_h d_v \times d_r}$ are learnable parameters, with $d_k = d_v = d_r/n_h$. Each head can learn to focus on different types of financial relationships. The output of the i -th head \mathbf{a}_i is:

$$\mathbf{a}_i = \text{softmax} \left(\frac{(\mathbf{Q}\mathbf{W}_i^Q)(\mathbf{K}\mathbf{W}_i^K)^\top}{\sqrt{d_k}} \right) (\mathbf{V}\mathbf{W}_i^V) \quad (3)$$

The outputs of all heads are then combined to produce the final MHA output:

$$\text{MHA}(\mathbf{Q}, \mathbf{K}, \mathbf{V}) = [\mathbf{a}_1; \dots; \mathbf{a}_{n_h}] \mathbf{W} \quad (4)$$

The full SA block uses a Pre-LayerNorm architecture for better training stability:

$$\mathbf{H}' = \mathbf{H}^{(l-1)} + \text{MHA}(\text{LN}(\mathbf{H}^{(l-1)}), \text{LN}(\mathbf{H}^{(l-1)}), \text{LN}(\mathbf{H}^{(l-1)})) \quad (5)$$

$$\mathbf{H}^{(l)} = \mathbf{H}' + \phi_{\text{ffn}}(\text{LN}(\mathbf{H}')) \quad (6)$$

where LN is Layer Normalization and ϕ_{ffn} is a feed-forward network.

After L layers, the final output $\mathbf{H}^{(L)}$ contains representations where each point is informed by the global market structure of that day.

3.1.2. Decoder

The decoder uses the contextualized representation $\mathbf{H}^{(L)}$ to predict the output distribution for any target coordinate $\tilde{\mathbf{x}}_j \in \mathcal{X}_T$. This is achieved by treating the decoding process as a query mechanism. First, each target coordinate is mapped to an initial query vector using the same positional encoding function:

$$\mathbf{z}_j^{(0)} = \gamma(\tilde{\mathbf{x}}_j) \quad (7)$$

These query vectors, forming the matrix $\mathbf{Z}^{(0)} = [\mathbf{z}_1^{(0)}, \dots, \mathbf{z}_M^{(0)}]^\top$, are then refined through a stack of L' cross-attention blocks (CA). The decoding process can be interpreted as using a target's location to query the rich, contextualized information database built from the observed data points. This allows each target point to aggregate the most relevant information for its own prediction. For each target, it computes a set of relevance scores against all points in the context set, effectively learning a unique set of weights for combining the context representations.

$$\mathbf{Z}^{(l)} = \text{CA}(\mathbf{Z}^{(l-1)}, \mathbf{H}^{(L)}) \quad \text{for } l = 1, \dots, L' \quad (8)$$

The CA block uses the MHA, where queries come from the target representations \mathbf{Z} and keys/values come from the context representation $\mathbf{H}^{(L)}$. The final target representations, $\mathbf{Z}^{(L')} = [\mathbf{z}_1^{(L')}, \dots, \mathbf{z}_M^{(L')}]^\top$, which contains all necessary information distilled from the context set for each specific target, are passed through a MLP, $\phi_d : \mathbb{R}^{d_r} \rightarrow \mathbb{R}^2$:

$$[\mu_j, \log \sigma_j^2]^\top = \phi_d(\mathbf{z}_j^{(L')}) \quad (9)$$

This yields the final predictive distribution $\mathcal{N}(\mu_j, \sigma_j^2)$ for the volatility at coordinate $\tilde{\mathbf{x}}_j$.

3.2. Training

Our model is trained using a meta-learning approach that comprises two distinct stages. The training process relies on two primary data sources.

3.2.1. Data Sources and Task Generation

The first data source is the collection of real market data, $\{\mathcal{D}_q\}_{q \in \mathcal{Q}}$, where $\mathcal{D}_q = \{(\mathbf{x}_j, y_j)\}_{j=1}^{N_q}$ is the set of all N_q observed option quotes for a given trading day q . The second is a synthetic dataset, $\{\hat{\mathcal{D}}_q\}_{q \in \mathcal{Q}}$, where $\hat{\mathcal{D}}_q$ is the corresponding dense, smooth volatility surface generated by a calibrated SABR model¹.

At each training step, a new task is generated. This process begins by randomly sampling a day index q from the set of available trading days \mathcal{Q} . Subsequently, a context set \mathcal{D}_C and a target set \mathcal{D}_T are constructed by drawing samples from the data sources \mathcal{D}_q and/or $\hat{\mathcal{D}}_q$, with the specific sampling strategy depending on the training stage.

3.2.2. Objective Function

The model's parameters θ are optimized by minimizing the negative log-likelihood (NLL) over the target sets. For a single task generated from day q , the loss is defined over its context set \mathcal{D}_C and target set $\mathcal{D}_T = \{(\tilde{\mathbf{x}}_j, \tilde{y}_j)\}_{j=1}^M$:

$$\mathcal{L}(\theta; \mathcal{D}_C, \mathcal{D}_T) = - \sum_{j=1}^M \log p_\theta(\tilde{y}_j | \mathcal{D}_C, \tilde{\mathbf{x}}_j) = \frac{1}{2} \sum_{j=1}^M (\exp(-\log \sigma_j^2) (\tilde{y}_j - \mu_j)^2 + \log \sigma_j^2) \quad (10)$$

In each training step, we sample a task and compute the gradient of this loss function.

3.2.3. Staged Meta-Learning

The training curriculum is a two-stage process designed to first instill a robust prior and then adapt it to market specifics.

- **Stage 1: Pre-training.** The goal of this stage is to instill a financial-theoretic prior into the model. For each task, a day q is sampled, and the context set \mathcal{D}_C is drawn from the sparse, real market quotes \mathcal{D}_q , while the target set \mathcal{D}_T is drawn from the corresponding dense, synthetic SABR surface $\hat{\mathcal{D}}_q$. The model's parameters θ are then updated by minimizing the loss $\mathcal{L}(\theta; \mathcal{D}_C, \mathcal{D}_T)$. This process encourages the model to learn a general mapping from partial, noisy observations to a globally coherent surface structure.

¹SABR is calibrated to each maturity slice in \mathcal{D}_q , and parameters are linearly interpolated across the term structure.

- **Stage 2: Fine-tuning.** This stage adapts the learned prior to real-world market dynamics. The model is initialized with the parameters $\theta = (\theta_{\text{enc}}, \theta_{\text{dec}})$ from the pre-training stage. For each task, a day q is sampled, and now both the context set \mathcal{D}_C and the target set \mathcal{D}_T are sampled exclusively from the real market data \mathcal{D}_q , ensuring the sets are non-overlapping. The optimization objective remains the loss $\mathcal{L}(\theta; \mathcal{D}_C, \mathcal{D}_T)$.

4. Experiments

4.1. Experimental Setup

Our experiments are carried out on a comprehensive dataset of S&P 500 (SPX) index options, spanning from January 2006 to August 2023. The raw data is from *OptionMetrics* dataset and is strictly partitioned by time to ensure a fair evaluation of model generalization. Data from 2006 to 2018 is used for training and validation, with 15% of the trading days randomly held out for validation. Data from 2019 to 2023 serves as the out-of-sample test set for all final evaluations. Quotes are preprocessed by computing mid-prices from best bid/ask, filter for basic liquidity. Forward prices are computed from the zero-coupon curve and dividend yields (OptionMetrics), and implied volatilities are obtained under the Black framework. Descriptive statistics of the dataset are in Table 1.

Table 1: Descriptive statistics of the dataset. The dataset is partitioned by time into a training & validation set and a test set.

Statistic	Category	Training & Validation Set	Test Set
Maturity	Short-Term ($\leq 3\text{M}$)	1,355,448 (75.0%)	1,723,463 (70.5%)
	Mid-Term (3M-1Y)	367,168 (20.3%)	633,933 (25.9%)
	Long-Term ($> 1\text{Y}$)	84,265 (4.7%)	88,796 (3.6%)
Moneyness	ATM ($ \log(K/F) \leq 0.05$)	903,275 (50.0%)	1,183,639 (48.4%)
	NTM ($0.05 < \log(K/F) \leq 0.2$)	747,269 (41.4%)	1,047,066 (42.8%)
	FTM ($ \log(K/F) > 0.2$)	156,337 (8.7%)	215,487 (8.8%)

We evaluate our proposed **VolNP-FT**² against an ablation version, **VolNP-Base**³ (trained only on real data), and three benchmarks. The benchmarks are: (1) a slice-calibrated **SABR** model⁴, (2) a **Gaussian Process (GP)** with an RBF kernel, and (3) a Surface SVI (**SSVI**) model⁵. For each test day, we uniformly sample a context set of $N = 100$ quotes from all available quotes of that day; the target set comprises the remaining quotes for that day. All baselines and VolNP variants are evaluated on the identical target sets. Performance is measured by Root Mean Squared Error (RMSE) and Mean Absolute Error (MAE). All error metrics are reported in basis points (BPS), where 1 BPS equals 0.01% in implied volatility.

4.2. Overall and Stratified Performance

Table 2 presents the main results. Overall, VolNP-FT achieves the best performance, with the lowest RMSE (99.60 BPS) and MAE (48.86 BPS). A key finding comes from the comparison with VolNP-Base. While their overall MAE is similar, the pre-training strategy allows VolNP-FT to reduce the RMSE by nearly 40%. This suggests that the SABR-induced prior does not just improve the average fit, but is particularly effective at preventing large, financially significant prediction errors.

²‘FT’ stands for ‘Fine-tuning’. The hidden dimension of VolNP models d_r is 128. Both the encoder and decoder MLPs (ϕ_e, ϕ_d) consist of 3 hidden layers with 128 units each and GELU activation. We use $L = 3$ self-attention blocks and $L' = 3$ cross-attention blocks, each with 4 attention heads.

³All models are trained with the AdamW optimizer. VolNP-FT is pre-trained for up to 200 epochs with a learning rate of 5×10^{-5} and fine-tuned for up to 100 epochs with a learning rate of 1×10^{-6} . The VolNP-Base model is trained for up to 300 epochs with a learning rate of 5×10^{-5} .

⁴SABR is calibrated to each maturity slice, and its parameters are linearly interpolated across the term structure.

⁵The SSVI model uses the arbitrage-free parameterization of Gatheral and Jacquier (2014). Its global parameters are calibrated to the entire context set for each day to ensure a surface free of static arbitrage.

Table 2: Overall and stratified performance comparison. Short-, mid-, and long-term correspond to maturities of 0-3 months, 3-12 months, and >12 months, respectively. All errors are in basis points (BPS). Best result in each category is in **bold**.

Model	Overall		Short-Term		Mid-Term		Long-Term	
	RMSE	MAE	RMSE	MAE	RMSE	MAE	RMSE	MAE
VolNP-FT	99.60	48.86	106.82	51.40	77.06	40.60	97.17	58.39
VolNP-Base	166.85	49.77	174.55	46.01	150.07	56.09	121.79	77.66
SABR	153.71	67.59	135.45	59.83	158.84	70.95	338.48	194.22
GP	274.90	73.84	58.53	32.62	255.10	78.69	1244.98	838.73
SSVI	248.46	174.26	219.45	155.14	260.27	192.15	531.22	417.38

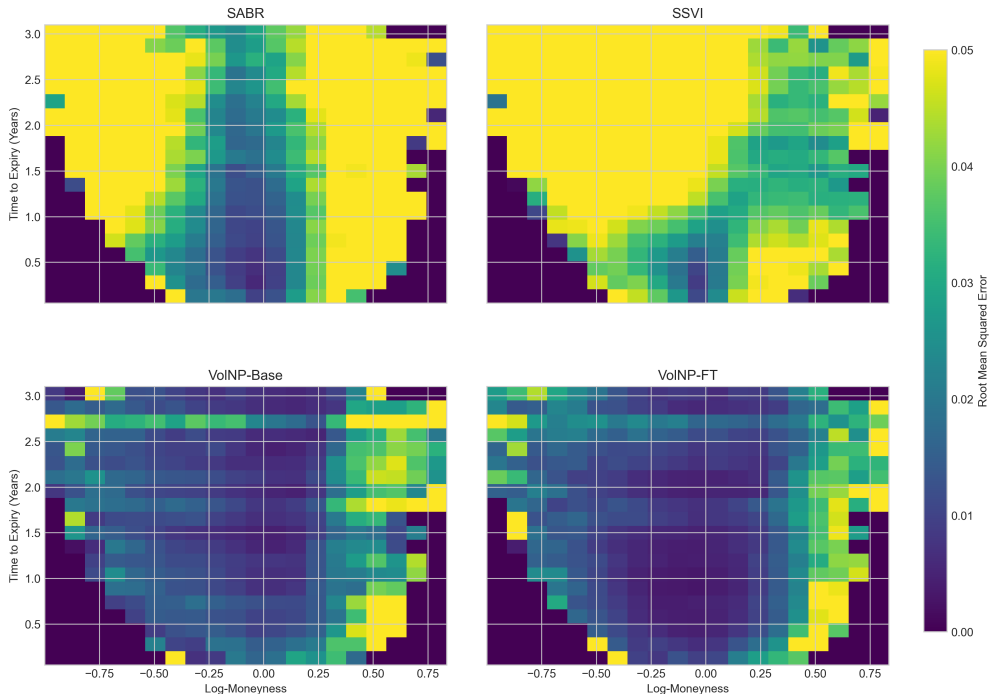


Figure 2: Root Mean Squared Error (RMSE) heatmaps for benchmark and VolNP models. Darker colors represent lower error.

The stratified results provide further insight. For short-term options, where market data is most dense, the flexible Gaussian Process model performs best. However, as maturity increases and data becomes sparser, the performance of GP and other benchmarks degrades. In these mid- and long-term regimes, VolNP-FT outperforms all other models. This indicates that the learned geometric prior is crucial for constructing a coherent and robust surface, especially in regions with fewer data points.

Figure 2 reveals the models' error patterns. Parametric models like SABR and SSVI show systematic errors on the 'wings' of the surface, whereas VolNP-FT demonstrates uniformly low error, indicating superior generalization. The comparison with VolNP-Base highlights that the SABR-based prior acts as a powerful regularizer, suppressing large errors and ensuring a more robust surface reconstruction.

4.3. Sensitivity to Data Sparsity

To study the robustness of the model, we examine the performance of model under variety data sparsity (Figure 3). The RMSE metric shows that VolNP-FT maintains a lower RMSE across all levels of sparsity, demonstrating data efficiency. VolNP-FT's lower RMSE confirms its ability to maintain a globally plausible surface shape instead of just fitting local points. This highlights its reliability for practical applications.

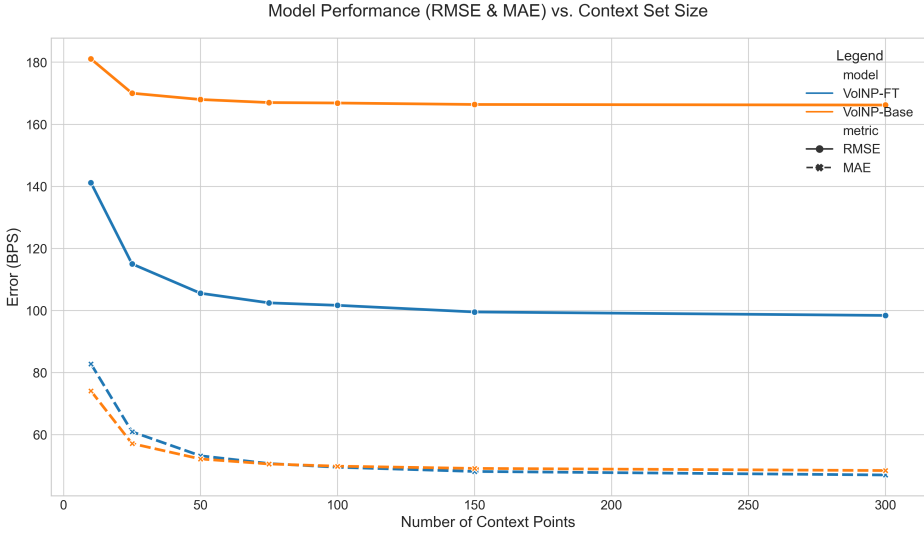


Figure 3: Model error (RMSE and MAE) as a function of the number of context points. VolNP-FT demonstrates superior data efficiency, achieving lower error with fewer context points and showing more stable performance as data becomes sparse.

4.4. Case Study: Surface Reconstruction Under Market Stress

We visualize the reconstructed surfaces on a challenging day: March 10, 2023, a day of significant market turmoil following the collapse of Silicon Valley Bank. This event provides a real-world stress test for model robustness. Figure 4 provides a comprehensive comparison, where each model reconstructs the surface from the same 100 context points drawn from the sparse market data (plotted as blue dots in panel a). Red dots in (a) are unobserved data to represent the ground truth.

The benchmark models exhibit distinct failure modes. The SABR model (b) produce a surface that is structurally plausible but overly rigid, failing to capture finer market details. The highly flexible Gaussian Process (c) overfits the sparse data, producing an unstable and financially implausible surface with unnatural oscillations. The ablation model VolNP-Base (e), while capturing some features of smiles, yields an irregular surface, suggesting it overfits local noise without a global structural guide. In contrast, VolNP-FT (f) reconstructs a surface that is successfully capturing the essential features of the ground truth market data. This visual evidence reinforces the quantitative results, suggesting that the geometric prior learned during pre-training is critical for regularizing the model and enabling it to generate coherent global structures from sparse local information.

A critical test for a model’s practical utility is the absence of butterfly arbitrage. We test for violations of the no-butterfly-arbitrage condition, which ensures the model’s implied risk-neutral probability density is non-negative. This test is performed by checking the Durrleman condition (further details, see Theorem 2.9, condition IV3 of (Roper, 2010)). Figure 5 shows the result on March 10, 2023. Smiles from VolNP-Base (bottom row) exhibit significant violations of this condition, indicated by the red shaded areas where arbitrage opportunities exist. This makes the model unusable in practice. In contrast, smiles from VolNP-FT (top row) are consistently free of such arbitrage. This shows that our two-stage training successfully provide a structural prior that guides the model to produce outputs that adhere to fundamental financial principles.

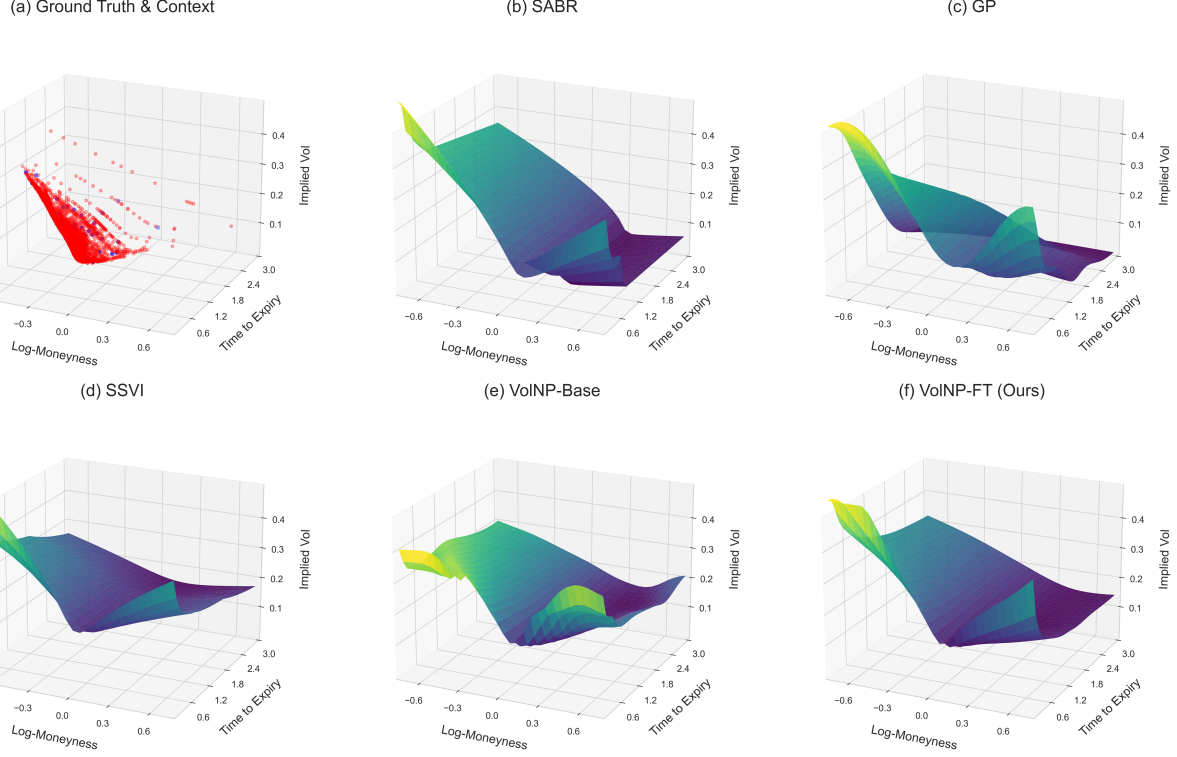


Figure 4: Implied volatility surface construction on March 10, 2023. Each model attempts to reconstruct the full surface from the same context dots (blue dots) shown in (a). Red dots in (a) are unobserved data to represent the ground truth.

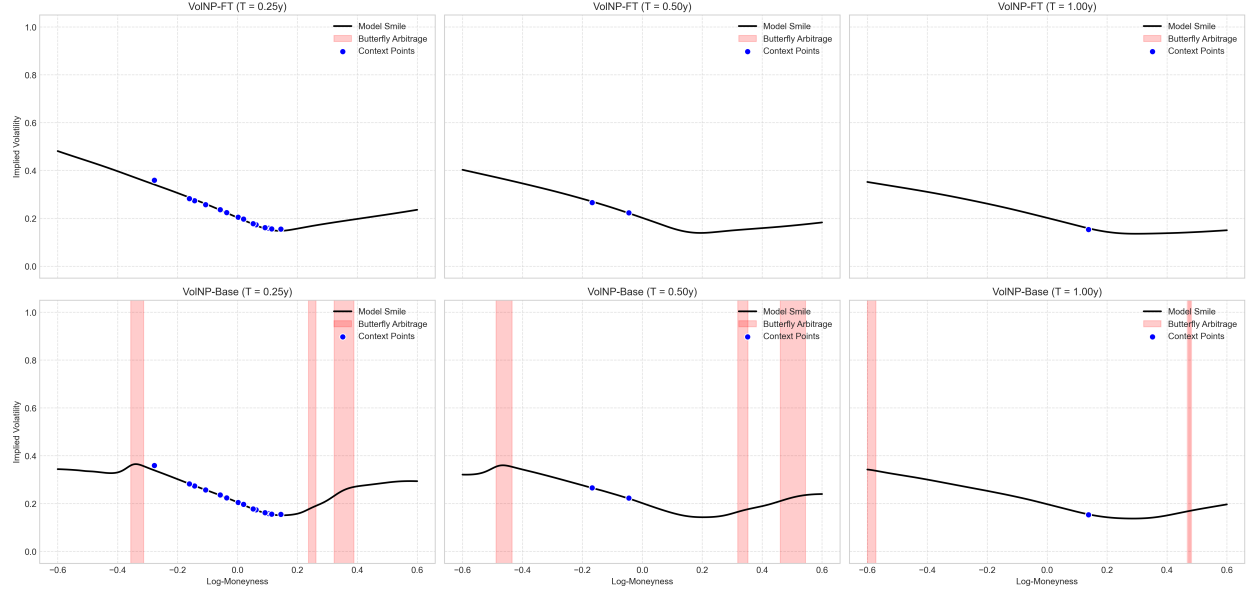


Figure 5: Arbitrage analysis on March 10, 2023. The red shaded areas indicate regions where the smile is admitting butterfly arbitrage (against Durrleman condition).

5. Conclusion

Traditional methods for constructing the implied volatility surface often treat each trading day as an isolated calibration task. This paper explores an alternative approach by framing surface construction as a meta-learning task. We propose the Volatility Neural Process, a model designed to learn a general mapping from sparse option quotes to a complete implied volatility surface. The model is first pre-trained on SABR-generated data to learn a financial-theoretic prior, and subsequently fine-tuned on market data to capture real-world dynamics. By learning the general task of surface construction, this framework yields a single model that does not require daily re-calibration, offering a potentially more efficient and reliable solution for constructing the implied volatility surface.

Empirical results on the SPX options dataset indicate that this approach is effective. The proposed model outperforms the considered benchmarks in overall accuracy and demonstrates robustness to data sparsity. The analysis also confirms that the pre-training stage is crucial for reducing large errors and for generating surfaces that are free from butterfly arbitrage.

References

Ackerer, D., Tagasovska, N., Vatter, T., 2020. Deep smoothing of the implied volatility surface, in: Proceedings of the 34th International Conference on Neural Information Processing Systems, Curran Associates Inc., Red Hook, NY, USA.

Chataigner, M., Cousin, A., Crépey, S., Dixon, M., Gueye, D., 2021. Beyond surrogate modeling: Learning the local volatility via shape constraints. *SIAM Journal on Financial Mathematics* 12, SC58–SC69.

Chen, H., Cheng, Y., Liu, Y., Tang, K., 2023. Teaching economics to the machines. Available at SSRN 4642167.

De Spiegeleer, J., Madan, D.B., Reyners, S., Schoutens, W., 2018. Machine learning for quantitative finance: fast derivative pricing, hedging and fitting. *Quantitative Finance* 18, 1635–1643.

Garnelo, M., Rosenbaum, D., Maddison, C., Ramalho, T., Saxton, D., Shanahan, M., Teh, Y.W., Rezende, D., Eslami, S.A., 2018a. Conditional neural processes, in: International conference on machine learning, PMLR. pp. 1704–1713.

Garnelo, M., Schwarz, J., Rosenbaum, D., Viola, F., Rezende, D.J., Eslami, S., Teh, Y.W., 2018b. Neural processes. ICML Workshop on Theoretical Foundations and Applications of Deep Generative Models .

Gatheral, J., 2004. A parsimonious arbitrage-free implied volatility parameterization with application to the valuation of volatility derivatives. Presentation at Global Derivatives & Risk Management, Madrid , 0.

Gatheral, J., Jacquier, A., 2014. Arbitrage-free svi volatility surfaces. *Quantitative Finance* 14, 59–71.

Hagan, P., Kumar, D., Lesniewski, A., Woodward, D., 2002. Managing smile risk. *Wilmott Magazine* 1, 84–108.

Heston, S.L., 1993. A closed-form solution for options with stochastic volatility with applications to bond and currency options. *The review of financial studies* 6, 327–343.

Hoshisashi, K., Phelan, C.E., Barucca, P., 2023. No-arbitrage deep calibration for volatility smile and skewness. arXiv preprint arXiv:2310.16703 .

Kim, H., Mnih, A., Schwarz, J., Garnelo, M., Eslami, A., Rosenbaum, D., Vinyals, O., Teh, Y.W., 2019. Attentive neural processes, in: Proceedings of the International Conference on Learning Representations (ICLR).

Roberts, S., Tegnér, M., 2021. Probabilistic machine learning for local volatility. *Journal of Computational Finance* 25.

Roper, M., 2010. Arbitrage free implied volatility surfaces. preprint .

Vaswani, A., Shazeer, N., Parmar, N., Uszkoreit, J., Jones, L., Gomez, A.N., Kaiser, L., Polosukhin, I., 2017. Attention is all you need. *Advances in neural information processing systems* 30.

Vuletić, M., Cont, R., 2024. Volgan: a generative model for arbitrage-free implied volatility surfaces. *Applied Mathematical Finance* 31, 203–238.

Wiedemann, R., Jacquier, A., Gonon, L., 2025. Operator deep smoothing for implied volatility, in: The Thirteenth International Conference on Learning Representations (ICLR).

Xiong, R., Yang, Y., He, D., Zheng, K., Zheng, S., Xing, C., Zhang, H., Lan, Y., Wang, L., Liu, T., 2020. On layer normalization in the transformer architecture, in: *Proceedings of the International Conference on Learning Representations (ICLR)*.

Zheng, Y., Yang, Y., Chen, B., 2021. Incorporating prior financial domain knowledge into neural networks for implied volatility surface prediction, in: *Proceedings of the 27th ACM SIGKDD Conference on Knowledge Discovery & Data Mining*, pp. 3968–3975.